Pergamon

Int. J. Heat Mass Transfer. Vol. 37, No. 14, pp. 1985–2006, 1994

0017-9310/94 $7.00+0.00

0017-9310(94)E0056-Z

Numerical and experimental study of mixed and forced convection in a junction

J. C. ROY and C. BERTRAND
Institut de Génie Energétique, 2, Avenue Jean Moulin, 90000 Belfort, France

and

G. LE PALEC
Université Aix-Marseille II, Unité lasers de puissance, Institut Méditerranéen de Technologie, Technopôle de Château-Gombert, 13451 Marseille Cedex 20, France

(*Received* 24 *February* 1994)

Abstract—This paper presents a theoretical and experimental investigation of the laminar steady 2D-mixing flow in a junction. The numerical method developed by Gosman *et al.* has been applied to derive velocities and temperatures profiles in the mixing zone. The effects of the angle between the two branches of the junction and the air-flow rate upon the structure flow are analysed, for both forced and mixed convection cases. The experimental procedure is based upon a flow visualization technique and L.D.V. velocity measurements: a reasonably good agreement between theoretical and experimental results is found.

1. INTRODUCTION

BECAUSE OF its biochemical applications such as the study of blood flow in human vessels and engineering applications such as ventilation systems, the interaction of two forced flows in a junction has been the subject of a few works in the past 20 years. As summarized in refs. [1, 2], several flow configurations are possible, but most of the published reports treat tee junctions and dividing flows.

Some numerical investigations have been devoted to this problem: Blowers [3] examined the case of two-dimensional mixing and dividing flows in a tee junction whereas Pollard [2] treated the three-dimensional case for both laminar and turbulent flows. Some authors such as Bramley and Sloan [4] have studied the effect of the angle between the two branches of the junction for a two-dimensional laminar dividing flow. In this paper, the size of the recirculating zones which develop downstream of the junction was investigated. More recently, Hayes and Nandakumar [5] have undertaken a study of the mixed convection in a vertical planar tee branch. This work is also devoted to the dividing flow case and the results show the influence of the Reynolds and Grashof numbers on the structure flow.

From an experimental point of view, the dividing forced flow case has been studied by many investigators because of its biomechanical applications (see for example refs. [6, 7]). In these studies, only the structure flow is investigated. For the mixing flow case, Karino *et al.* [8] have performed a flow visualization in order to show how the two streams interact whereas Sparrow and Kemink [9] and Kawashima [10] measured the local Nusselt number downstream the mixing region. They found a substantial increasing of the heat transfer coefficient in this region.

For the problem of mixing flow and low velocities (laminar flow), the free convective effects cannot be neglected when a constant heat flux is specified on the walls of the mixing zone, the temperature of the fluid in the two entrance zones being the same. Except for a first approach by the present authors [11], a survey of the literature shows that free and forced convection heat transfer with mixing flows in branching systems has not yet been studied. This is the subject of this paper in which the theoretical analysis allows us to show the effects of the air-flow rate and the angle between the two branches of the junction upon the structure flow, for both forced and mixed convection cases. An experimental procedure based upon a flow visualization technique and L.D.V. velocity measurements provides a comparison with these theoretical results.

2. PROBLEM STATEMENT AND GOVERNING EQUATIONS

The physical model is shown in Fig. 1: the fluid is introduced through branches 1 and 2, respectively,

NOMENCLATURE

a	thermal diffusivity of the fluid [$m^2\ s^{-1}$]	v	Oy velocity component [$m\ s^{-1}$]
g	gravitational acceleration [$m\ s^{-2}$]	x, y	dimensional coordinates [m]
H	height of the exit branch (along y axis) [m]	X, Y	dimensionless coordinates.
K	ratio: (air flow rate in branch 2)/ (air flow rate in branch 1)		
p	pressure [$N\ m^{-2}$]	Greek symbols	
Pr	Prandtl number	α	angle between the two inlet branches [°]
q	intensity of the wall heat flux (mixed convection case) [$W\ m^{-2}$]	β	coefficient of thermal expansion [K^{-1}]
Re	Reynolds number	θ	dimensionless temperature
Ri	Richardson number	λ	thermal conductivity of the fluid [$W\ m^{-1}\ K^{-1}$]
T	temperature of the fluid [K]	ν	kinematic viscosity of the fluid [$m\ s^{-2}$]
T_0	temperature of the fluid on sections AB and GH (Fig. 1) [K]	ρ	density of the fluid [$kg\ m^{-3}$]
ΔT	difference $(T-T_0)$ [K]	ϕ	stream function [$m^2\ s^{-1}$]
u	Ox velocity component [$m\ s^{-1}$]	ψ	dimensionless stream function
U_0	mean velocity in the exit branch [$m\ s^{-1}$]	ω	vorticity [t^{-1}]
		Ω	dimensionless vorticity.

before interacting and exiting through the main branch 3. The cross-section of the inlet branches is S/2 and the angle between them, noted α, may vary from 1 to 90°. Boundary conditions are fixed by assuming a fully developed flow in the inlet and outlet sections (AB, HG and DE, respectively). The length of the exit branch, CE, is deduced in order to verify this assumption and its cross-section is S, so that the mean velocity remains constant. The walls of the junction may be subjected to various thermal conditions which will be developed later. Consideration is given to a steady laminar two-dimensional flow with constant physical properties, except for the density changes which are modelled according to the Boussinesq approximation. Experiments showed that two-dimensionality is a good assumption if the distance between lateral walls of the channel is rather high. This assumption also allows to make some comparisons with previous published numerical results for some limiting cases. It can be noticed that there are many industrial codes that can handle this problem. However, these codes need a computer with very large memory capacities and such a computer was not available in our laboratory, so that it was necessary to perform a specific numerical procedure. A Cartesian coordinates system was chosen with u and v denoting

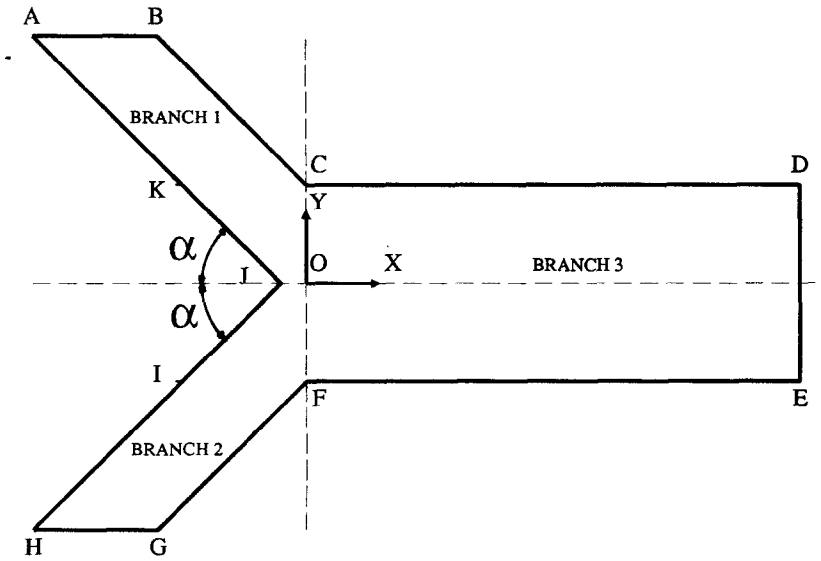

FIG. 1. Physical model and definition of the coordinates system.

the velocity components along Ox and Oy directions, respectively. Under the above assumptions, the continuity, Navier–Stokes and energy equations are:

$$\frac{\partial u}{\partial x}+\frac{\partial v}{\partial y}=0, \tag{1}$$

$$u\frac{\partial u}{\partial x}+v\frac{\partial u}{\partial y}=\nu\left(\frac{\partial^2 u}{\partial x^2}+\frac{\partial^2 u}{\partial y^2}\right)-\frac{1}{\rho}\frac{\partial p}{\partial x}, \tag{2}$$

$$u\frac{\partial v}{\partial x}+v\frac{\partial v}{\partial y}=\nu\left(\frac{\partial^2 v}{\partial x^2}+\frac{\partial^2 v}{\partial y^2}\right)-\frac{1}{\rho}\frac{\partial p}{\partial y}+g\beta\Delta T, \tag{3}$$

$$u\frac{\partial T}{\partial x}+v\frac{\partial T}{\partial y}=\nu\left(\frac{\partial^2 T}{\partial x^2}+\frac{\partial^2 T}{\partial y^2}\right), \tag{4}$$

where T is the temperature, p the pressure, ρ the density and β the coefficient of thermal expansion, ν and a being the kinematic viscosity and the thermal diffusivity of the fluid. By introducing the stream function ϕ and the vorticity ω, we get:

$$\frac{\partial^2\phi}{\partial x^2}+\frac{\partial^2\phi}{\partial y^2}=-\omega, \tag{5}$$

$$\frac{\partial\phi}{\partial y}\frac{\partial\omega}{\partial x}-\frac{\partial\phi}{\partial x}\frac{\partial\omega}{\partial y}=\nu\left(\frac{\partial^2\omega}{\partial x^2}+\frac{\partial^2\omega}{\partial y^2}\right)+g\beta\frac{\partial\Delta T}{\partial x}, \tag{6}$$

$$\frac{\partial\phi}{\partial y}\frac{\partial T}{\partial x}-\frac{\partial\phi}{\partial x}\frac{\partial T}{\partial y}=\nu\left(\frac{\partial^2 T}{\partial x^2}+\frac{\partial^2 T}{\partial y^2}\right), \tag{7}$$

with:

$$u=\frac{\partial\phi}{\partial y}\quad v=-\frac{\partial\phi}{\partial x}\quad \omega=\frac{\partial v}{\partial x}-\frac{\partial u}{\partial y}. \tag{8}$$

Let us now introduce the following dimensionless quantities:

$$X=\frac{x}{H}\quad Y=\frac{y}{H}\quad U=\frac{u}{U_0}\quad V=\frac{v}{U_0}$$

$$\psi=\frac{\phi}{U_0 H}\quad \Omega=\frac{\omega H}{U_0}\quad \theta=\frac{\lambda\Delta T}{qH}, \tag{9}$$

H, U_0 and λ being defined in the nomenclature. Equations (5)–(7) become:

$$\frac{\partial^2\psi}{\partial X^2}+\frac{\partial^2\psi}{\partial Y^2}=-\Omega, \tag{10}$$

$$\frac{\partial\psi}{\partial Y}\frac{\partial\Omega}{\partial X}-\frac{\partial\psi}{\partial X}\frac{\partial\Omega}{\partial Y}=\frac{1}{Re}\left(\frac{\partial^2\Omega}{\partial X^2}+\frac{\partial^2\Omega}{\partial Y^2}\right)+Ri\frac{\partial\theta}{\partial X}, \tag{11}$$

$$\frac{\partial\psi}{\partial Y}\frac{\partial\theta}{\partial X}-\frac{\partial\psi}{\partial X}\frac{\partial\theta}{\partial Y}=\frac{1}{Re\,Pr}\left(\frac{\partial^2\theta}{\partial X^2}+\frac{\partial^2\theta}{\partial Y^2}\right), \tag{12}$$

where Re, Pr and Ri are the Reynolds, the Prandtl and the Richardson numbers that are defined as:

$$Re=\frac{U_0 H}{\nu}\quad Pr=\frac{\nu}{a}\quad Ri=\frac{g\beta qH^2}{\lambda U_0^2}. \tag{13}$$

The boundary conditions are written by assuming a fully-developed laminar flow and therefore a parabolic velocity profile at the entrance sections AB and GH where the temperature of the fluid is known. At the exit section (DE), the derivatives of T, ψ and Ω with respect of X vanish because the flow is again fully developed, as pointed out in our assumptions. The no-slip condition is used on the walls and a constant heat flux q may be specified on the walls of the mixing zone. When no heat flux occurs, the walls are assumed to be adiabatic. We thus have:

(i) For the stream function ψ:

on AB:

$$\psi=\frac{2X^2}{K+1}\sin^2(\alpha)[6-8X\sin(\alpha)], \tag{14}$$

where K denotes the ratio between the air flow-rate in branch 2 and the air flow-rate in branch 1:

on GH:

$$\psi=\frac{2KX^2}{K+1}\sin^2(\alpha)[6-8X\sin(\alpha)], \tag{15}$$

on BCD:

$$\psi=\frac{\sin^2(\alpha)}{K+1}[3-2X\sin(\alpha)], \tag{16}$$

on EFG:

$$\psi=-\frac{K\sin^2(\alpha)}{K+1}[3-2X\sin(\alpha)], \tag{17}$$

on AH:

$$\psi=0, \tag{18}$$

on DE:

$$\frac{\partial\psi}{\partial X}=0. \tag{19}$$

(ii) For the vorticity:

on AB:

$$\Omega=-\frac{24}{K+1}[1-4X\sin(\alpha)], \tag{20}$$

on GH:

$$\Omega=\frac{24K}{K+1}[1-4X\sin(\alpha)], \tag{21}$$

on DE:

$$\frac{\partial\Omega}{\partial X}=0. \tag{22}$$

On the walls, Ω is numerically approximated by using the Woods method [12]: if M denotes a point of the wall, n and P being, respectively, the normal from the wall and a point that belongs to this normal, the vorticity at point M is:

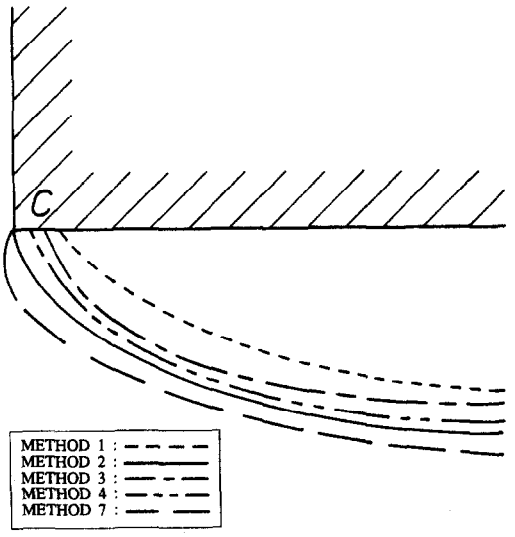

FIG. 2. Effect of the vorticity formulation on the shape of the recirculating zone near the corner: comparison between solutions proposed by Roache [13].

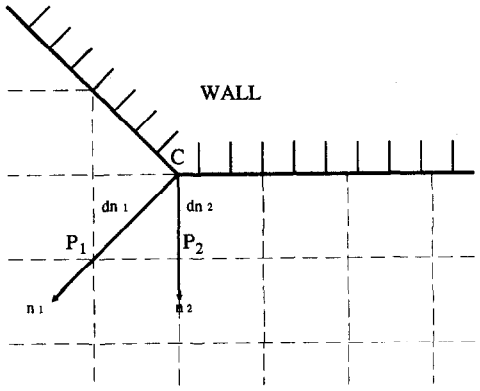

FIG. 3. Determination of the vorticity on the corners (point C or F).

$$\Omega_M = \frac{3(\psi_M - \psi_P)}{dn^2} - \frac{1}{2}\Omega_P + O(n^2) \qquad (23)$$

where dn is the distance MP. A better approximation is obtained by choosing a second point, R, located at the distance dm from the point M (with $dm > dn$). However, this may induce numerical instabilities as shown by Blowers [3]. The distances dn and dm also have an effect upon the convergence [12].

More difficulties are encountered for calculating Ω on the corners (i.e. on points C and F) because the vorticity becomes higher and higher near these points. For solving this problem, the seven methods proposed by Roache [13] have been tested with the following values: $Re = 500$, $K = 1$ and $\alpha = 90°$. The shape of the streamline $\psi = 0.5$, which stands for the limit of the recirculating zone near the corner C, is shown in Fig. 2. The seven methods are labelled as in the Roache reference. Methods 5 and 6 are not presented because they give $\Omega_C = 0$ and there is no recirculating zone downstream of the corner, which is physically false. Method 2 (continued line) has been selected because it is the one which gives a correct shape of the recirculating region, as it was experimentally observed. This method consists in calculating the vorticity from the two points P_1 and P_2 (Fig. 3), by means of equation (23), and then adding them.

(iii) For the temperatures, we have $\theta = 0$ on sections AB and GH. If the walls are adiabatic, then we set $\theta_M = \theta_P$. If a wall heat flux q is specified, the dimensionless thermal boundary condition is:

$$\theta_M = \theta_P + \frac{dn}{H}. \qquad (24)$$

Finally, on DE we have:

$$\frac{\partial \theta}{\partial X} = 0. \qquad (25)$$

3. NUMERICAL METHOD

For solving equations (10)–(12) subjected to the boundary conditions (14)–(25), the finite difference procedure of Gosman *et al.* [14] (upwind difference technic) has been applied. Note that the choice of the Cartesian coordinate system allows to remain unchanged the grid system in the exit branch, which facilitates the comparison between all the results. Examples of grid systems are shown in Figs. 4 and 5 for $\alpha = 45$ and $\alpha = 90°$, respectively. For saving accuracy of the results, a greater grid density is specified near the walls and in the mixing region. As noted above, the derivatives of θ, ψ and Ω with respect of X must vanish at the section DE: this condition was used to calculate the length of the main branch so that this length did not affect the results.

The discretized equations were solved with the Gauss–Seidel method. All the calculations were performed with an accuracy of the solutions less than 10^{-5}, the relaxation factor being 10^{-2} for the vorticity and 1 for the stream function and the temperature. For these conditions and a Reynolds number less than 500, convergence was reached with approximately 1000 iterations. Note that results obtained for $Re > 500$ are not presented in this study because experiments showed that the flow in the exit branch then becomes turbulent, so that the laminar flow assumption fails.

The numerical procedure was tested by calculating well-known flow problems such as, for instance, the flow in a plane channel with a constant velocity field at the entrance section: at the exit section, the flow was again fully developed and the discrepancy between numerical and exact solution was less than 1%. It also should be noted that calculations were performed in order to verify that no false diffusion occurred in the numerical procedure.

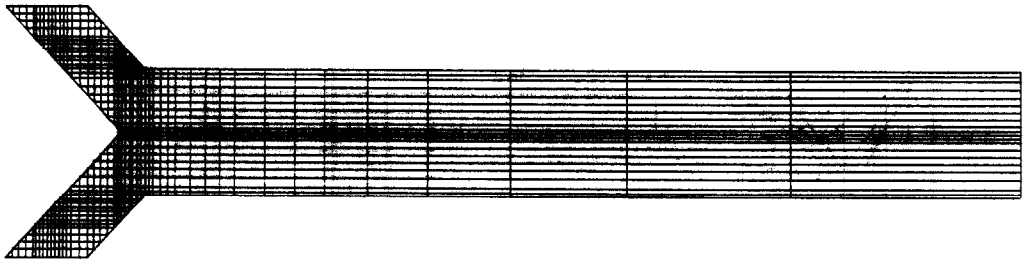

FIG. 4. Finite difference discretization for $\alpha = 45°$ of the interacting zone.

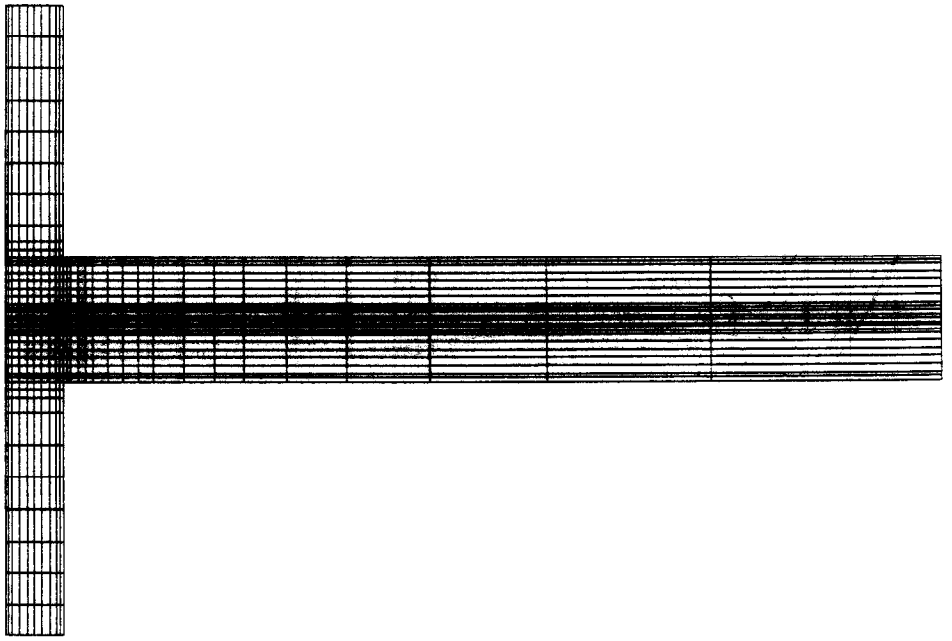

FIG. 5. Finite difference discretization for $\alpha = 90°$ of the interacting zone.

4. NUMERICAL RESULTS AND DISCUSSION

Numerical results were carried out for a Prandtl number of 0.7 (air) with Richardson numbers varying from 0 (pure forced convection case) to 20 (mixed convection). The mixed convection regime can result from the heating of the junction walls. This heating can be performed either on the surface limited by points I and K (Fig. 1) or on the upper and lower walls of the main branch. These two cases were chosen because they correspond to the way by which the walls are heated by a laser sheet during the flow visualization (see Section 5): they will be discussed in Section 3.2. Other parameters of greatest interest are the angle α and the ratio of inlet air flow-rates, K.

3.1. *Effect of the angle α and the ratio* K

We first present the results for pure forced convection case ($Ri = 0$). Four values of α (30, 45, 60 and 90°) and four flowing configurations have been tested:

(i) $Re = 100$ with $K = 1$;
(ii) $Re = 500$ with $K = 1$;
(iii) $Re = 150$ with $K = 2$; and
(iv) $Re = 300$ with $K = 5$.

For $K = 1$ and α less than 45°, there is no recirculating zone downstream of the corners (i.e. points C and F in Fig. 1). Such a recirculating zone appears when α and K increase. When K becomes higher, the recirculating zone develops downstream of the corner corresponding to the inlet branch in which the mean velocity is higher. Figures 6 and 7 show the streamlines for $\alpha = 60°$ and cases (iii) and (iv) above mentioned. The size of the recirculating zone at the bottom of the main branch is an increasing function of the Reynolds number, ratio K and angle α. If follows that the flow coming from the upper inlet branch is forced against the wall CD and so its mean velocity increases. For $\alpha = 90°$, two others recirculating zones which are symmetrical with respect to the OX axis occur against the IK section wall, which induces an acceleration of the flow near the corners: the results obtained for $\alpha = 90°$ can be found in ref. [11] and so they will not be repeated here. In Figs. 8–11, the local velocity profiles for two sections of the main branch ($X = 2$ and $X = 5$) are reported. These figures correspond to case (ii) (Figs. 8 and 9) and case (iv) (Figs. 10 and 11), respectively. For comparison, the Poiseuille velocity profile resulting from the laminar flow between two parallel

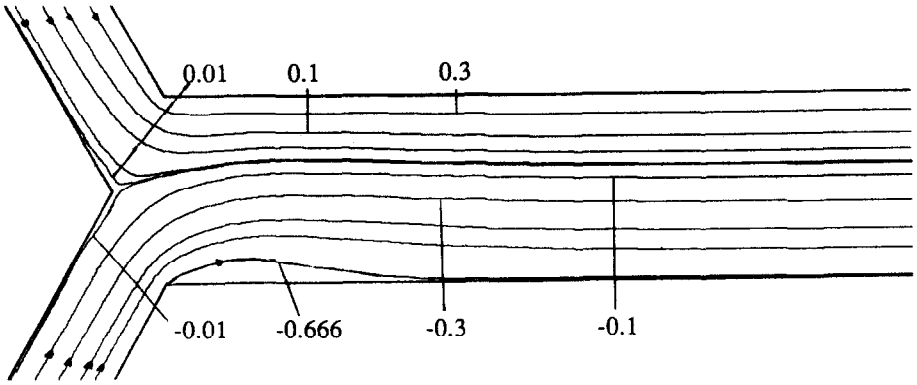

FIG. 6. Pure forced convection case: streamlines for $\alpha = 60°$, $Re = 150$, $K = 2$.

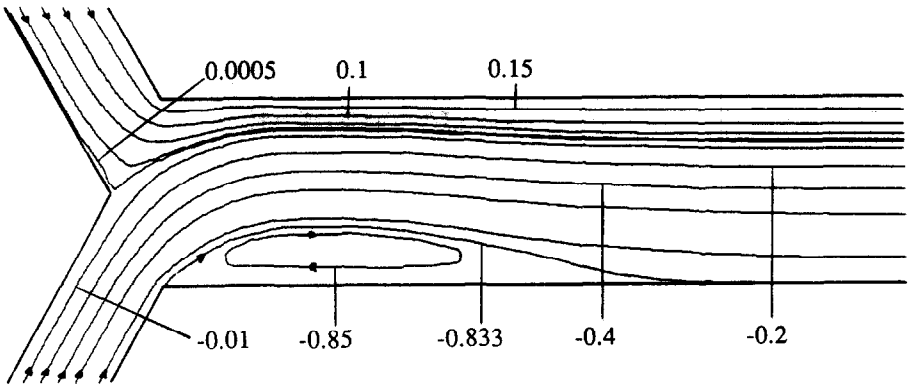

FIG. 7. Pure forced convection case: streamlines for $\alpha = 60°$, $Re = 300$, $K = 5$.

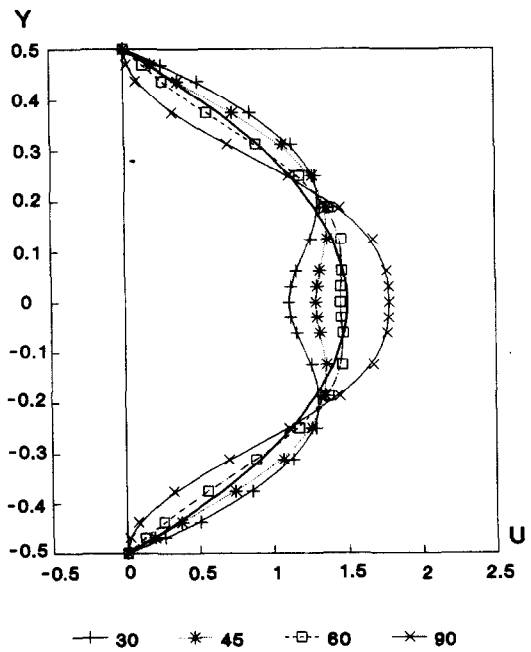

FIG. 8. Pure forced convection case: axial velocity profiles for $X = 2$, $Re = 500$, $K = 1$.

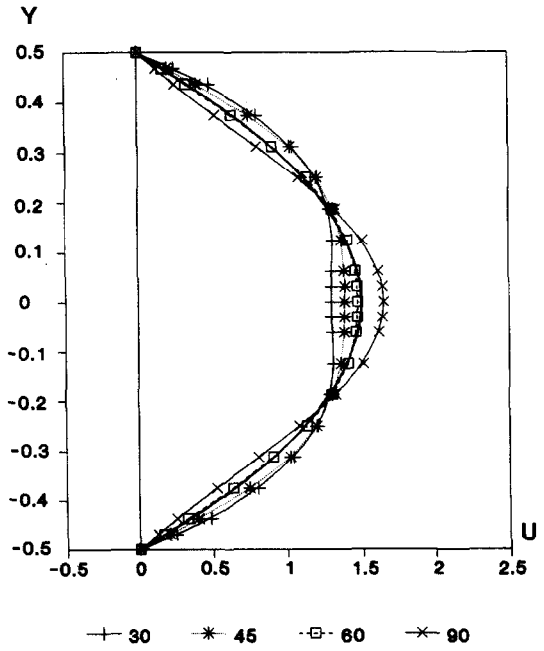

FIG. 9. Pure forced convection case: axial velocity profiles for $X = 5$, $Re = 500$, $K = 1$.

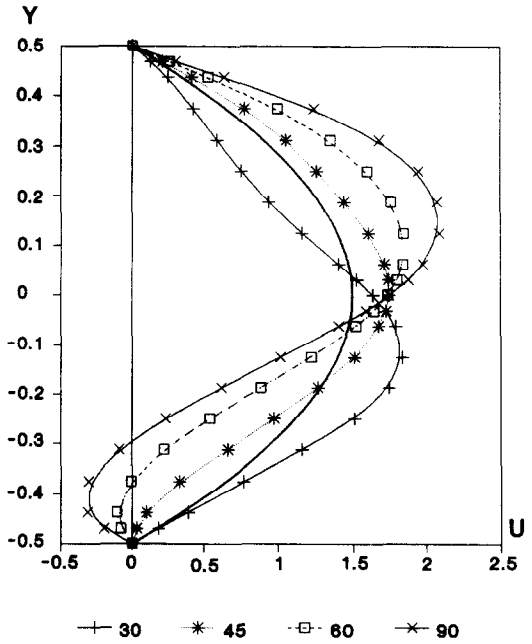

FIG. 10. Pure forced convection case: axial velocity profiles for $X = 2$, $Re = 300$, $K = 5$.

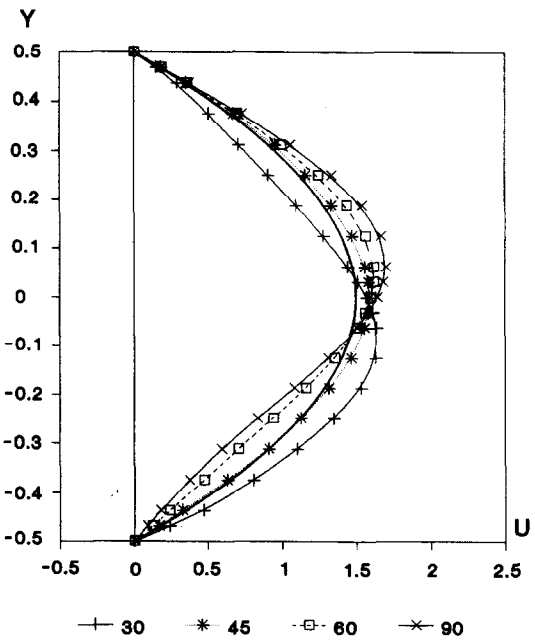

FIG. 11. Pure forced convection case: axial velocity profiles for $X = 5$, $Re = 300$, $K = 5$.

plates has also been drawn in bold line on each figure. When there is no recirculating zone, as for case (i), or when the size of the recirculating zones is small, we see that high values of the angle α aids the flow to be again fully developed in the exit branch. On the other hand, the flow becomes fully developed for higher and higher values of X as the size of the recirculating zone grows, as for the flow configurations (ii) and (iv).

3.2. *Effect of the mixed convection*

The mixed convection flow can be generated by heating the walls of the mixing junction. Two cases have been examined:

Case i: the section IK (see Fig. 1) is heated and all other walls of the mixing zone are adiabatic.

Case ii: the sections CD and FE are heated and all other walls of the mixing zone are adiabatic.

For case i, Figs. 12 and 13 show the effect of the Richardson number ($Ri = 5$ and $Ri = 20$) on the streamlines and the isotherms in the mixing zone of a tee branch. The values of the other parameters are $Re = 500$ and $K = 1$. As Ri increases, the fluid coming from the lower inlet branch moves higher and higher along the IK section of the wall, before interacting with the upper inlet stream and then being forced towards the main branch. As compared to the pure forced convection case ($Ri = 0$), this new structure also has an effect upon the velocity profiles in the mixing zone: velocities are higher in the upper part of the main branch and smaller in the lower region, which implies greater and smaller sizes of the recirculating zones, respectively. Figure 14 shows the changing streamlines and isotherms for a lower value of the Reynolds number ($Re = 100$). The size of recirculating zones is then reduced as compared to the previous case. Figures 15 and 16 show the mixed convection structure flow for $Re = 500$ and $\alpha = 60$ and 45°, respectively. As seen from these figures, the flow becomes less and less disturbed when α decreases. For $\alpha = 30°$, the structure is the same as for the pure convection case and, consequently, the corresponding figure has not been reported here. It should be noticed that the tested values of the wall heat flux are rather low, according with the laminar flow assumption and the assumed boundary conditions at the entrance sections: indeed, even for low values of α, a large wall heat flux evidently would have a noticable effect on the flow structure and would generate a turbulent flow, which is not considered in this study. Finally, it also should be noticed that the Nusselt number cannot be defined for this case of wall heating, because of the impossibility to define a mean temperature for constant Y.

When the heating is applied on the two walls of the exit branch (case ii) the main resulting effect is the changing of the size of upper and lower recirculating zones which, respectively, become greater and smaller than for pure forced convection flow. For such thermal conditions a Nusselt number can be defined as follows:

$$Nu_X = \frac{1}{\theta_{PX} - \theta_{MX}} \tag{26}$$

where θ_{PX} is the dimensionless wall temperature and θ_{MX} is the dimensionless mean temperature at the section X. For a fully developed flow, the theoretical value of the Nusselt number is $Nu_d = 8.235$ [16].

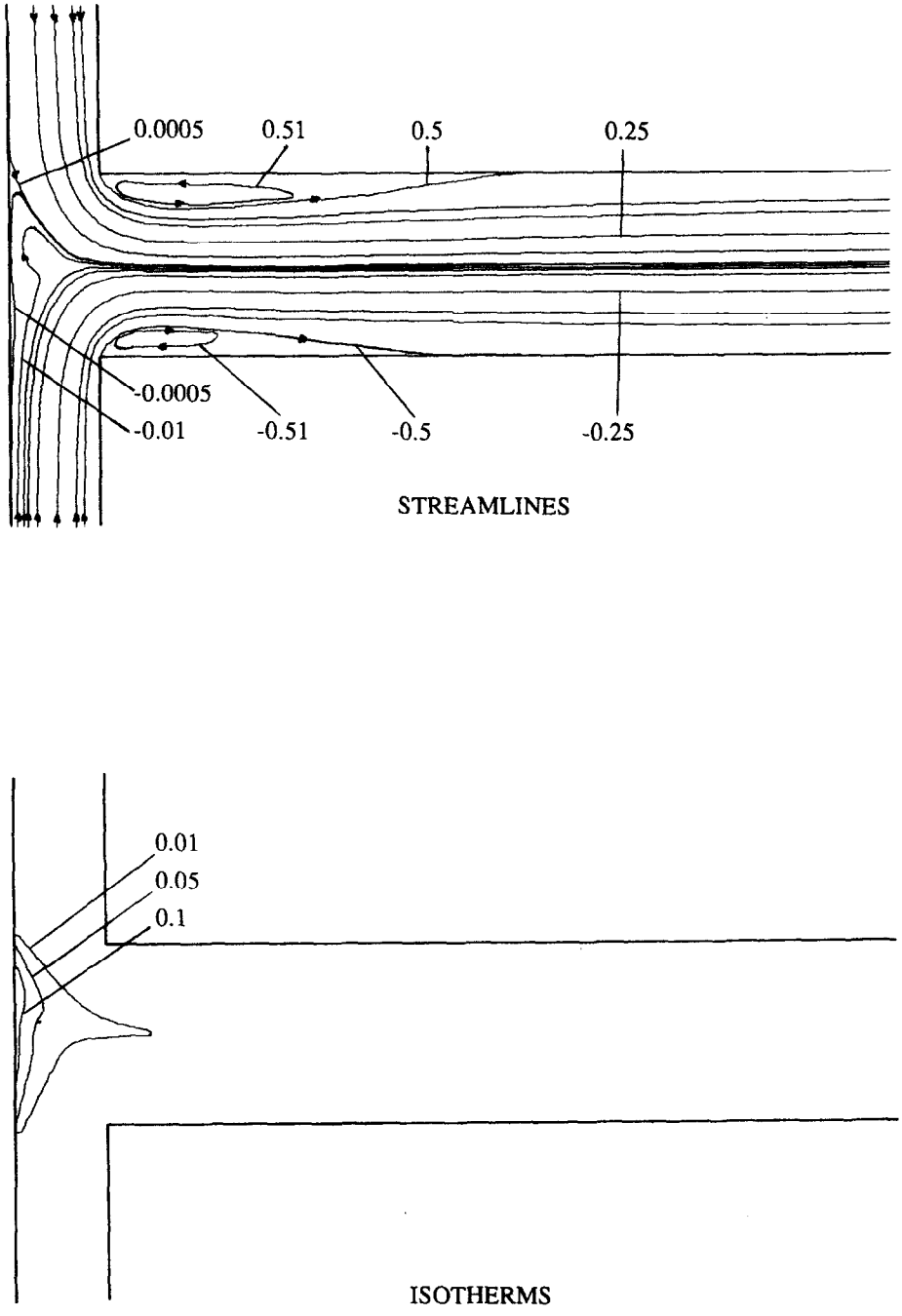

FIG. 12. Mixed convection case (case i) : streamlines and isotherms for $Ri = 5$, $\alpha = 90°$, $Re = 500$, $K = 1$.

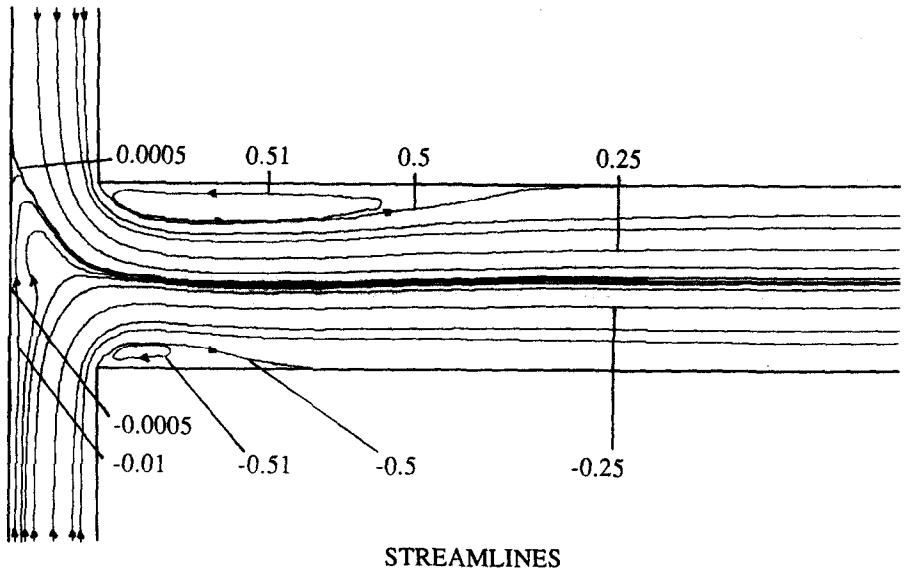

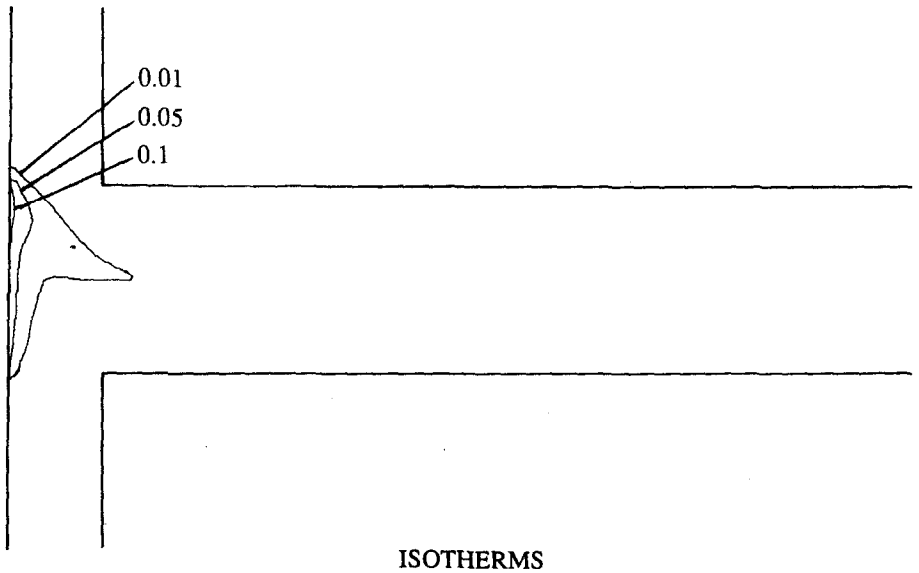

FIG. 13. Mixed convection case (case i) : streamlines and isotherms for $Ri = 20$, $\alpha = 90°$, $Re = 500$, $K = 1$.

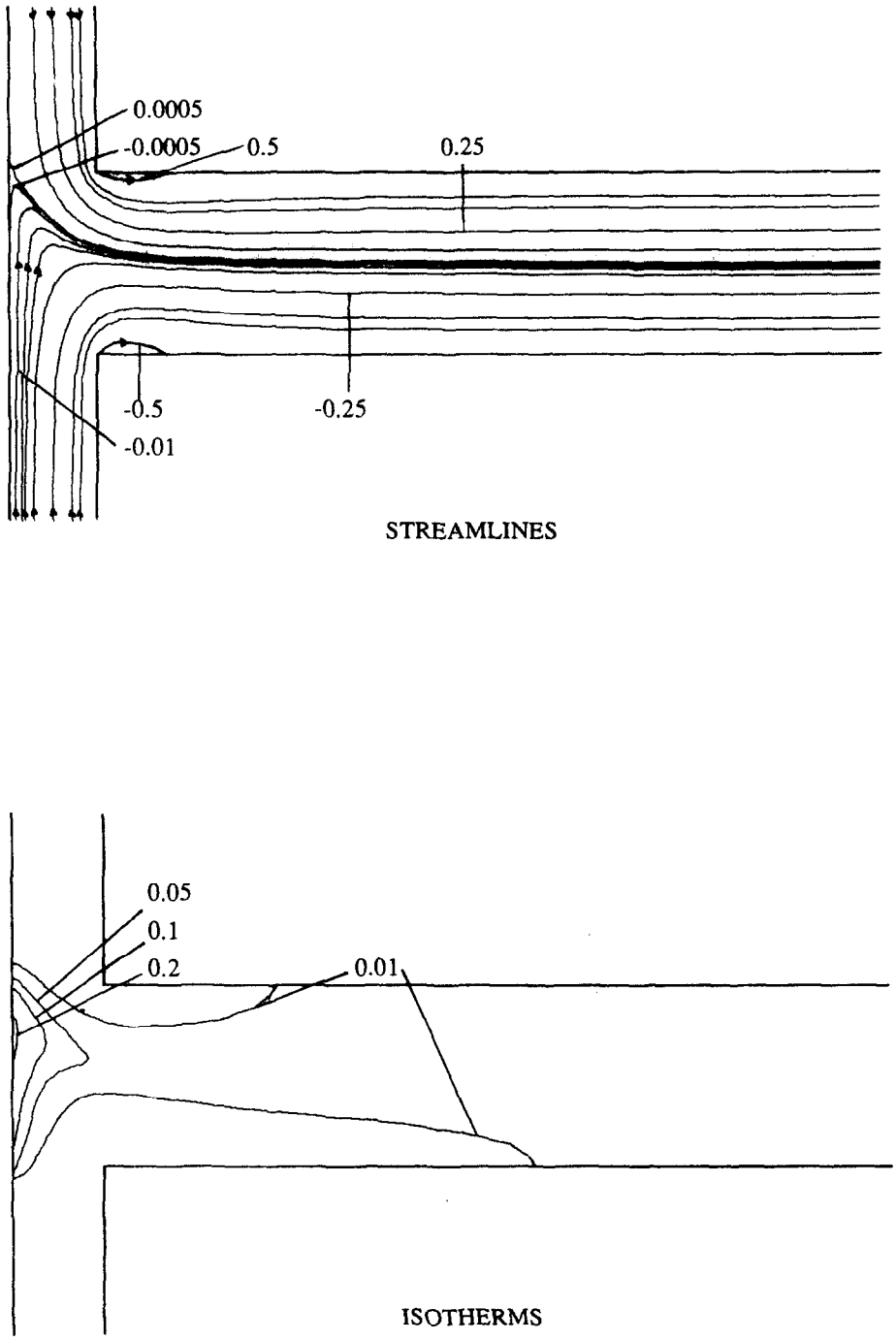

FIG. 14. Mixed convection case (case i) : streamlines and isotherms for $Ri = 20$, $\alpha = 90°$, $Re = 100$, $K = 1$.

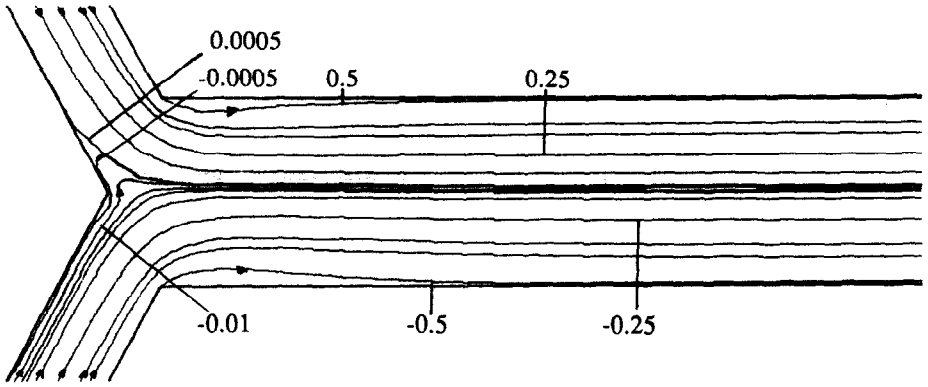

STREAMLINES

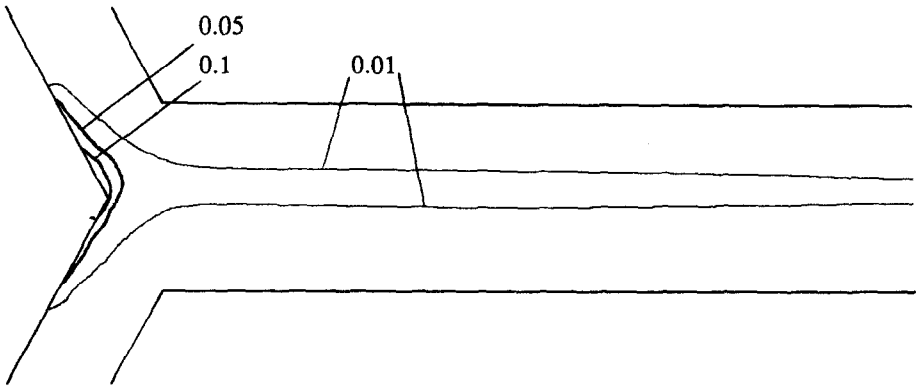

ISOTHERMS

FIG. 15. Mixed convection case (case i) : streamlines and isotherms for $Ri = 20$, $\alpha = 60°$, $Re = 500$, $K = 1$.

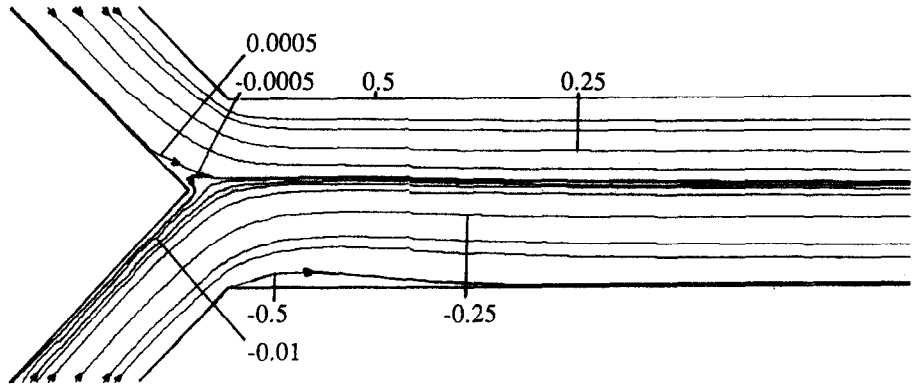

STREAMLINES

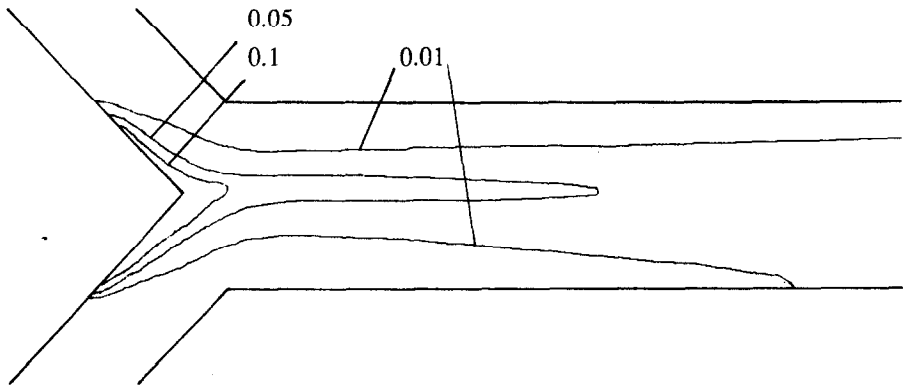

ISOTHERMS

FIG. 16. Mixed convection case (case i) : streamlines and isotherms for $Ri = 20$, $\alpha = 45°$, $Re = 500$, $K = 1$.

Figures 17–20 show the modification of the flow structure for $Re = 500$, $Ri = 20$, $K = 1$ and α varying from 30 to 90°. As α increases, the size of the recirculating zone which occurs against the upper wall increases whereas the lower wall's one decreases, as compared to the pure forced convection case. It has been verified that this phenomenon is an increasing function of the Richardson number. For $K = 1$, $Re = 100$ and 500, $Ri = 5$ and 20, the variations of the ratio between the local Nusselt number and Nu_d have been reported on Fig. 21 ($\alpha = 60°$) and Fig. 22 ($\alpha = 90°$). For each case, the values obtained on upper and lower walls have been plotted. This ratio is equal to unity at the exit section, which means that the flow is again fully developed, whereas it is greater than 1 in the recirculating zone: it follows that the mixing of the fluid increases the local heat transfer coefficient as it was earlier mentioned by Sparrow and Kemink [9] and Kawashima [10]. For $\alpha = 90°$ and for high Reynolds numbers, the local heat transfer coefficient first decreases and increases before again decreasing and becoming equal to 1: this is an effect of the higher size of the recirculating zones which then highly disturb the flow.

5. EXPERIMENTAL PROCEDURE

5.1. *Flow visualization*

In order to validate the numerical results, a visualization of the flow in the junction was performed in order to get some qualitative comparisons. The experimental apparatus is shown on Fig. 23: the air comes from a compressor before being extended and passing through two flowmeters which allow the adjustment and measurement of the air-flow rate in each entrance branch, the cross-section of which being 40×80 mm. The two flows are homogenized in tanks and then are moved towards the mixing zone which is made with altuglass. After interacting, the air is extracted through the main branch. The cross-section and length of the exit flow branch are 80×80 and 1000 mm, respectively. The optical apparatus for visualizations is realized with a 3 W Argon laser source and a spherico-cylindrical telescope [15] which allows the generation of a focused laser sheet at the middle of the interacting zone. This sheet is introduced by the air exit section of the main branch. Some tracers (oil particles) are introduced in the lower homogenization tank, so that the flow coming from this tank appears as white on the views. The density of tracers is adjustable as a function of the air-flow rate. Data acquisition is performed by means of a C.C.D. video camera.

Figures 24–27 present views of the flow structure in the interacting zone, as function of the angle α and the Reynolds number ($Re = 100$ and $Re = 500$), with $K = 1$ for all cases. When $\alpha = 30°$ (Fig. 24) and $\alpha = 45°$ (Fig. 25), the two flows remain separated and there is no recirculating zone in the exit branch. Two recirculating zones appear on the upper and lower walls of the exit branch for $\alpha = 60°$ (Fig. 26) and $\alpha = 90°$ (Fig. 27). The size of these zones is larger as the angle α and the Reynolds number increase. It is noticed that the upper recirculating zone appears as white on the views, which means that the air moving in it contains tracers and that it comes from the lower entrance branch. This is a consequence of lateral wall effects in the mixing region: it has been verified that the flow at the middle of the mixing zone is not disturbed by this phenomenon. It is also seen that, for $\alpha = 90°$ and for high Reynolds numbers (Fig. 27b), two vortices are created on the left wall: these vortices are symmetrical about the X direction. On the other hand, the vortices do not exist when the Reynolds number is low because, as seen from Fig. 27a, the air coming from the lower entrance ducts grows along the left wall before exiting. This flow structure is a mixed convection regime one, according with the numerical results of the previous paragraph. This regime is induced by the heating of the wall due to the laser sheet. The mixed convective flow is also observed for $\alpha = 60°$ (Fig. 26a), but it does not occur for $\alpha = 45°$ and $\alpha = 30°$, because the laser sheet is more and more reflected as the angle α decreases, which leads to a decreasing of the wall heating.

5.2. *Velocity measurements*

The same experimental bench was used in order to perform velocity measurements by means of the L.D.V. technique and so to provide a quantitative comparison with theory. Measures were made at several sections ($X = 2$ and $X = 5$) of the exit branch for several values of the angle α and the Reynolds number Re. Comparisons of these results with the numerical results are reported on Figs. 28–30. Figures 28 and 29 show the velocity profile for low values of α (30° and 45°) and $Re = 500$. For $X = 2$, the shape of the profile exhibits the two recirculating zones and the discrepancy between theoretical and experimental results is no more than 10%. The viscous effects seem to be over estimated in the numerical model and consequently the length of the mixing zone is slightly higher as compared to experiments. For $X = 5$, the flow is again fully developed and the discrepancy between theory and experiments is lower. For higher values of the angle α (60° and 90°), the comparison is also very good, as shown on Fig. 30 which presents the experimental and theoretical velocity profiles for $X = 5$ and $Re = 100$.

6. CONCLUSION

In this paper, we have presented a numerical study, visualizations and experimental velocity profiles of the forced and mixed laminar convection regimes in a branching system with mixing flow, the fluid being extracted through the main branch. The mixed convection regime is induced by heating the walls of the mixing zone. The theoretical analysis shows the effects of the angle between the two branches of the junction and the air-flow rate upon the structure flow. For the

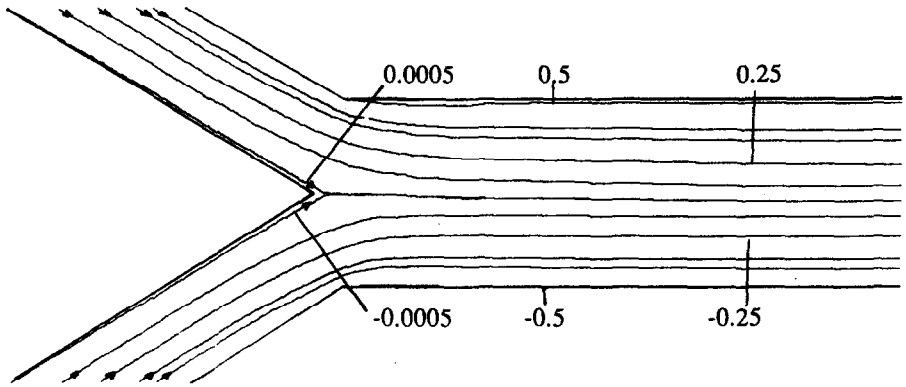

STREAMLINES

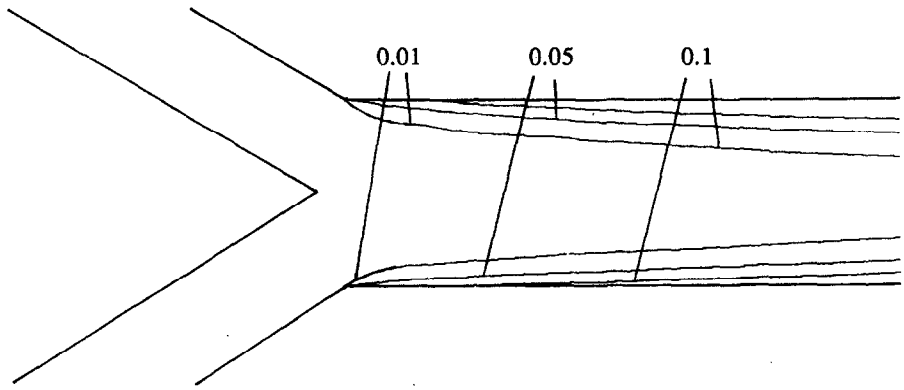

ISOTHERMS

FIG. 17. Mixed convection case (case ii) : streamlines and isotherms for $Ri = 20$, $\alpha = 30°$, $Re = 500$, $K = 1$.

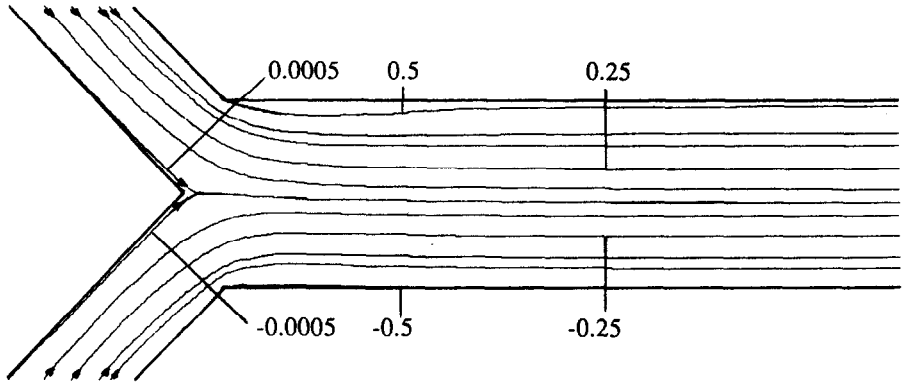

STREAMLINES

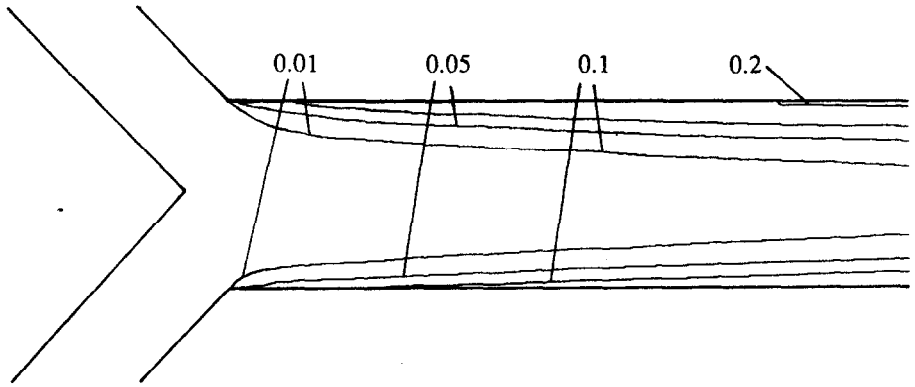

ISOTHERMS

FIG. 18. Mixed convection case (case ii) : streamlines and isotherms for $Ri = 20$, $\alpha = 45°$, $Re = 500$, $K = 1$.

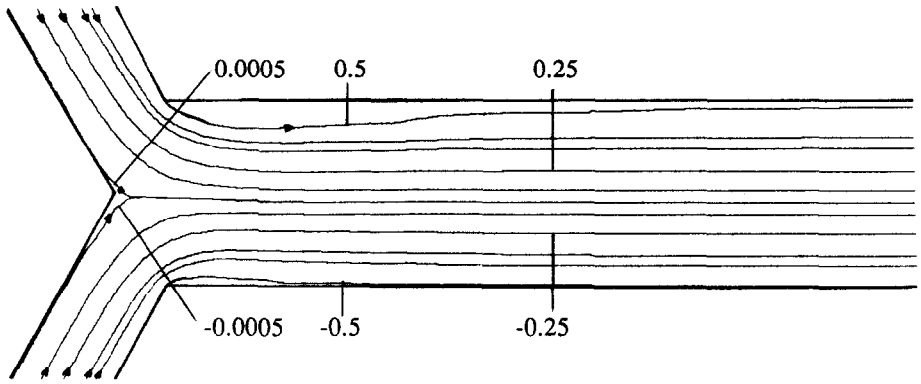

STREAMLINES

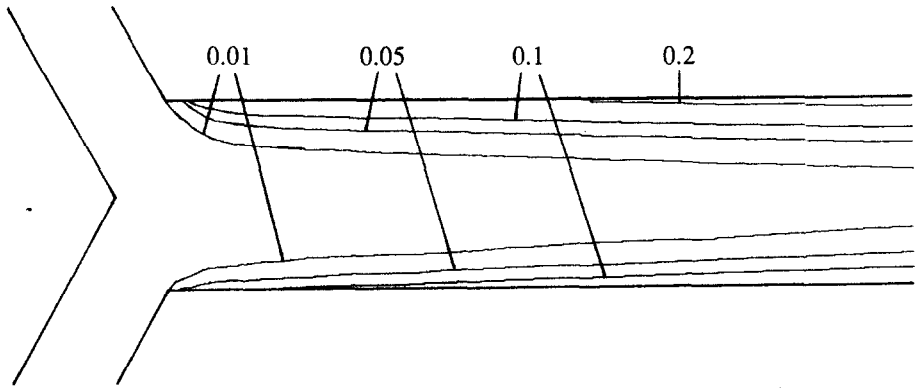

ISOTHERMS

FIG. 19. Mixed convection case (case ii) : streamlines and isotherms for $Ri = 20$, $\alpha = 60°$, $Re = 500$, $K = 1$.

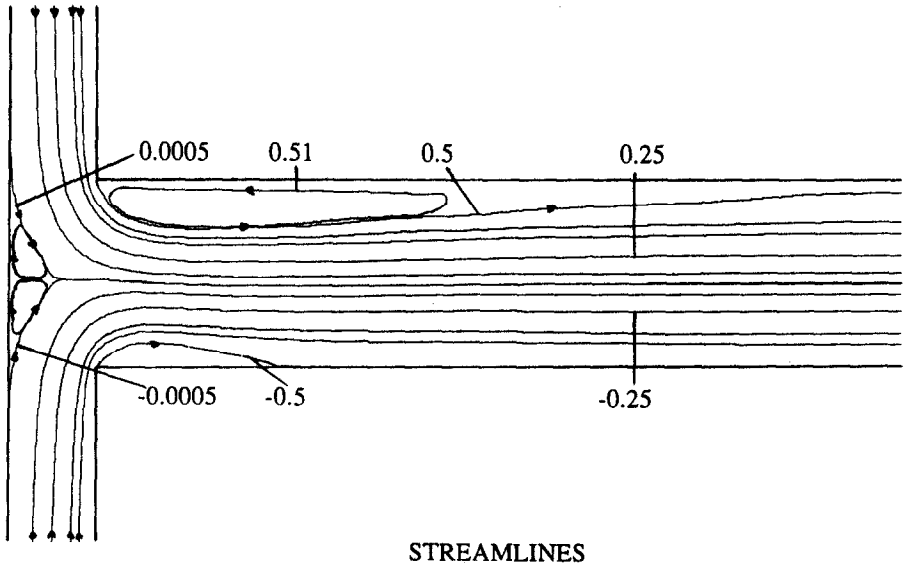

STREAMLINES

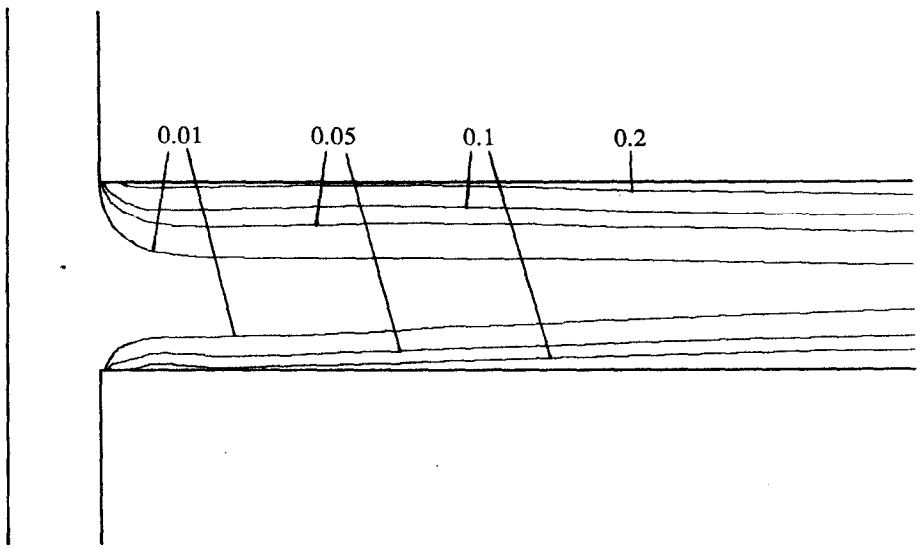

ISOTHERMS

FIG. 20. Mixed convection case (case ii) : streamlines and isotherms for $Ri = 20$, $\alpha = 90°$, $Re = 500$, $K = 1$.

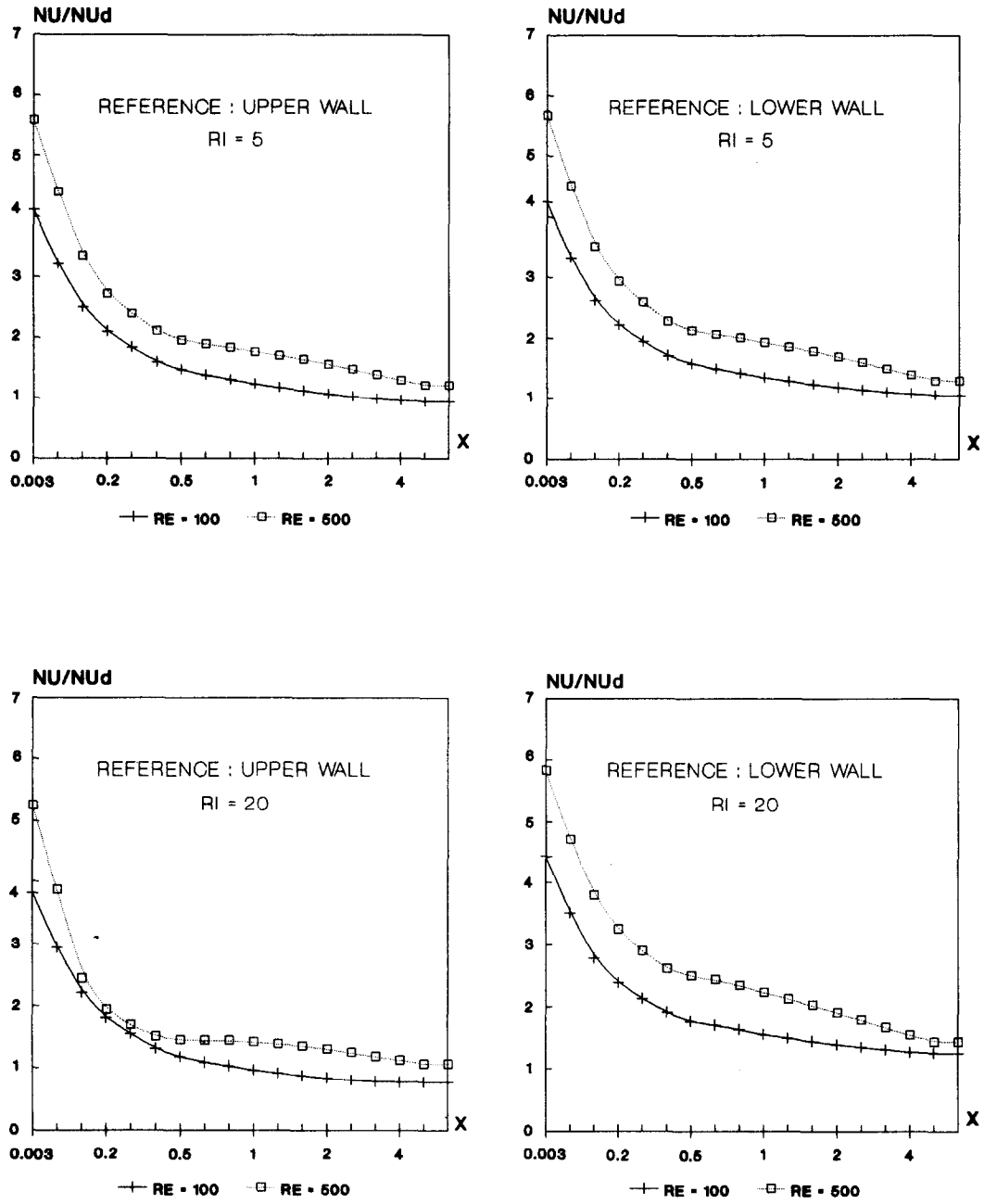

FIG. 21. Mixed convection case (case ii): Nu_X/Nu_d ratio as function of X for $Ri = 5$ and 20, $\alpha = 60°$, $Re = 100$ and 500, $K = 1$.

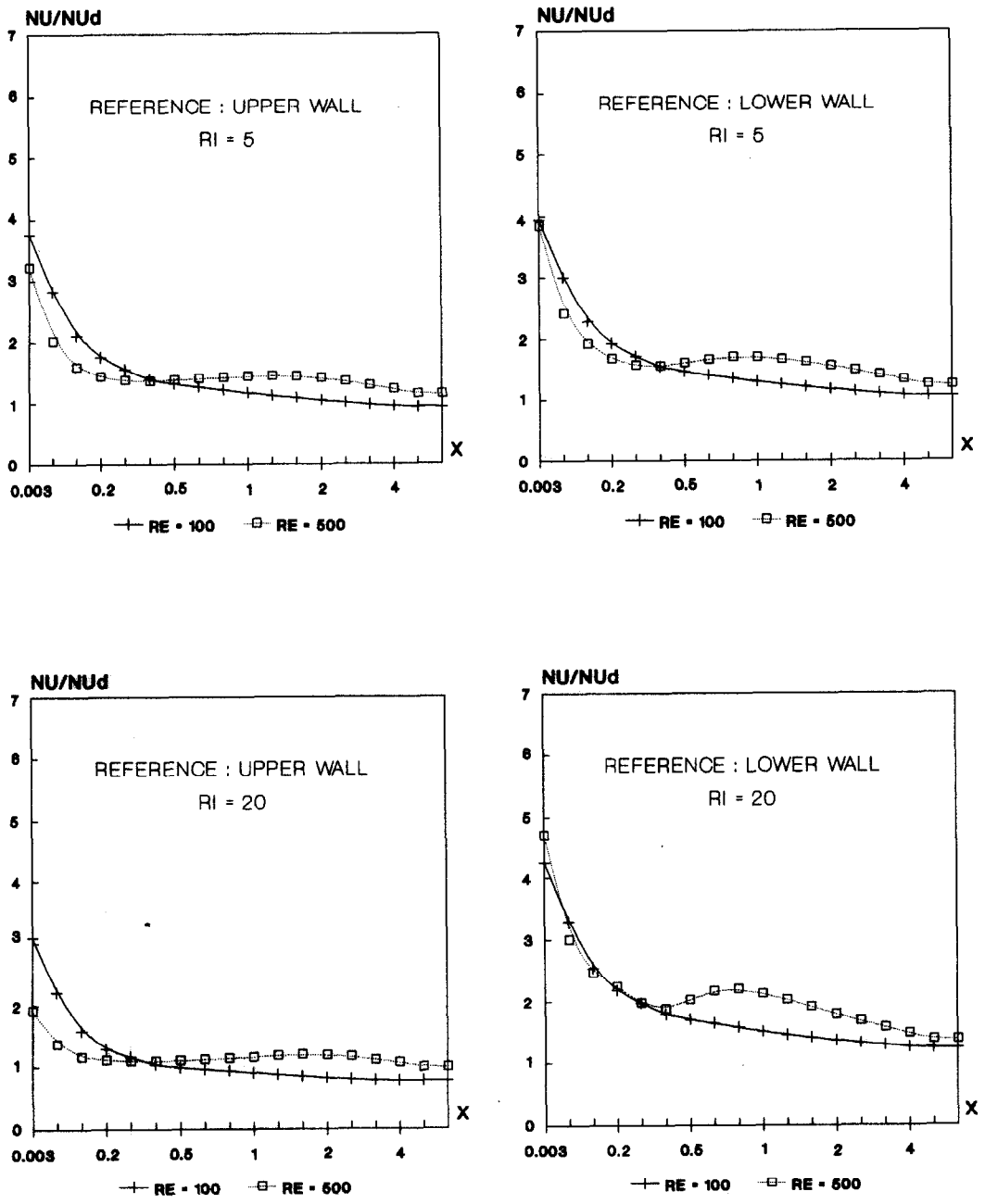

FIG. 22. Mixed convection case (case ii): Nu_X/Nu_d ratio as function of X for $Ri = 5$ and 20, $\alpha = 90°$, $Re = 100$ and 500, $K = 1$.

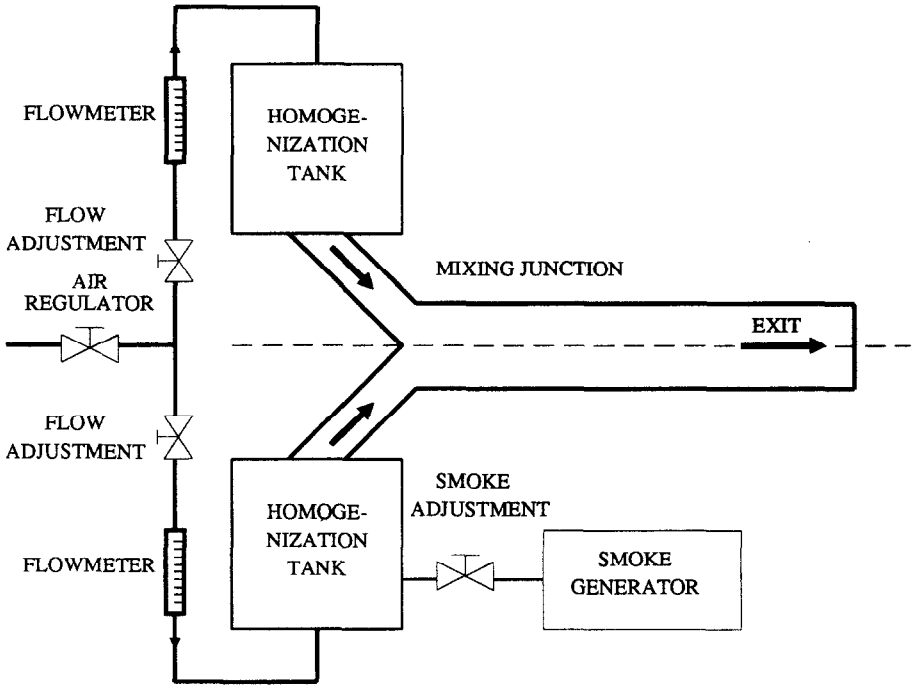

FIG. 23. Experimental apparatus for flow visualizations.

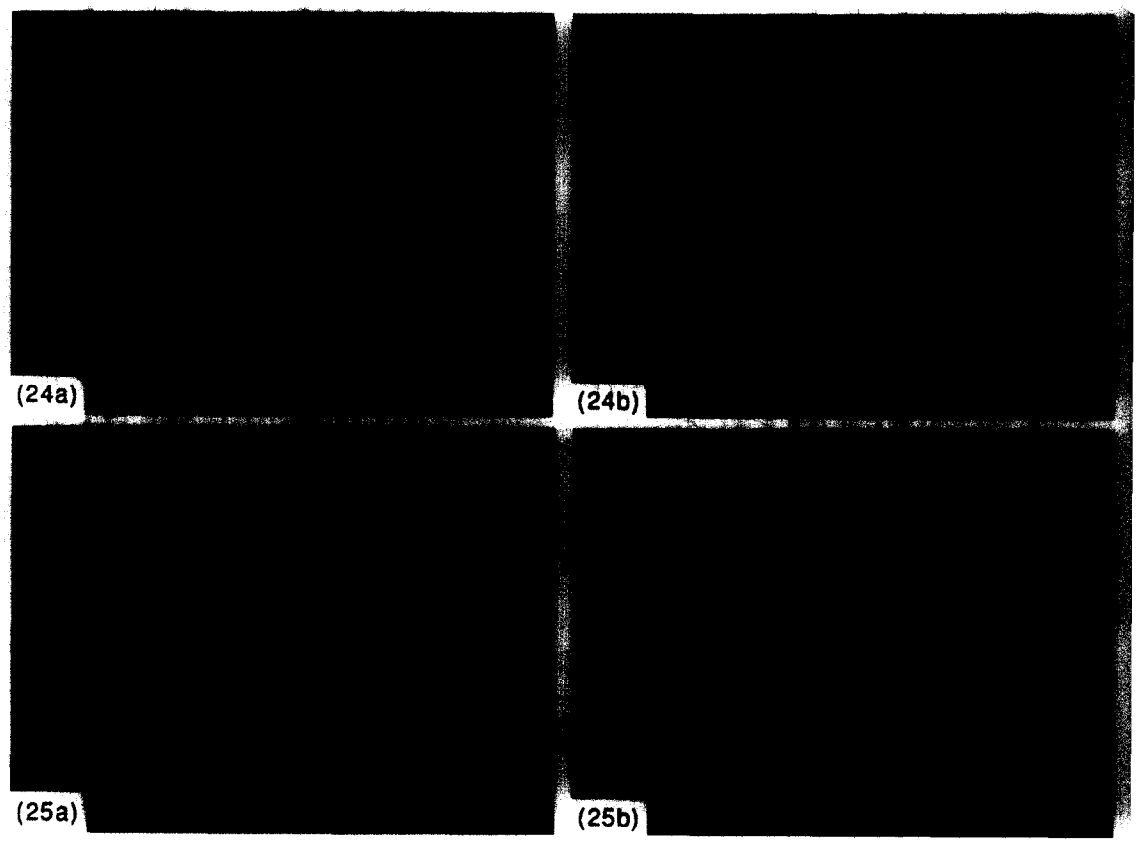

FIG. 24. Flow structure for $\alpha = 30^\circ$ and $Re = 100$ (a) and $Re = 500$ (b).

FIG. 25. Flow structure for $\alpha = 45^\circ$ and $Re = 100$ (a) and $Re = 500$ (b).

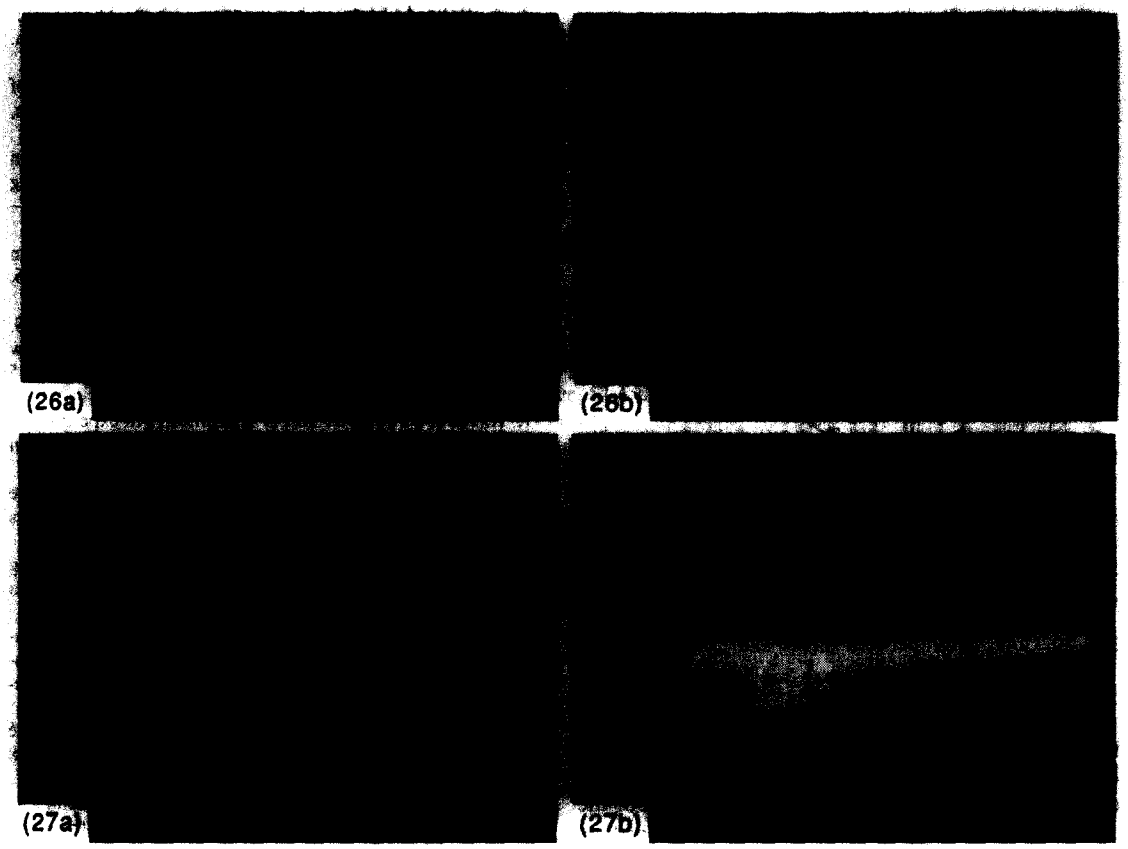

FIG. 26. Flow structure for $\alpha = 60°$ and $Re = 100$ (a) and $Re = 500$ (b).

FIG. 27. Flow structure for $\alpha = 90°$ and $Re = 100$ (a) and $Re = 500$ (b).

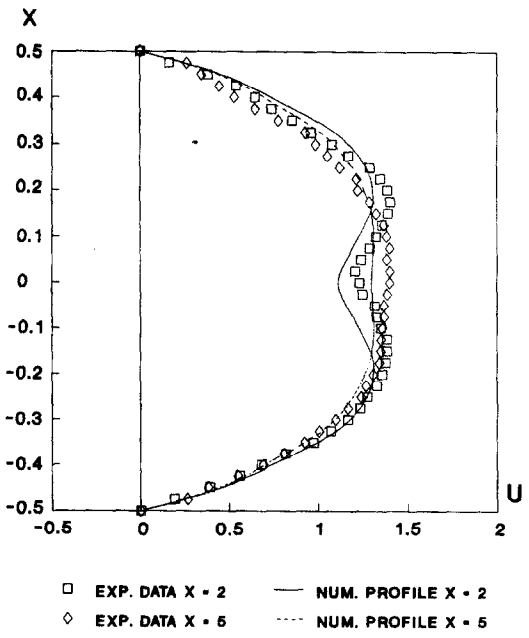

FIG. 28. Comparison between theory and L.D.V. measurements for $\alpha = 30°$ and $Re = 500$, $X = 2$ and $X = 5$.

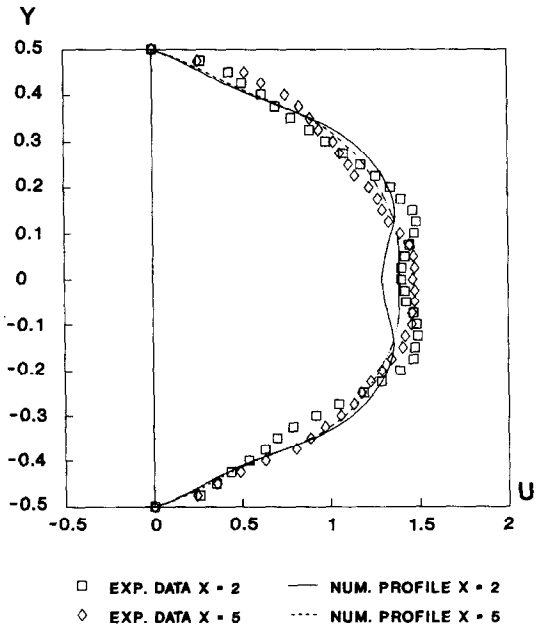

FIG. 29. Comparison between theory and L.D.V. measurements for $\alpha = 45°$ and $Re = 500$, $X = 2$ and $X = 5$.

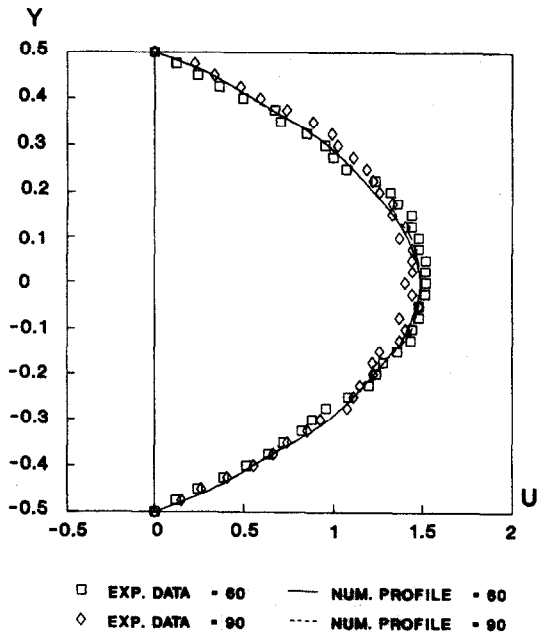

FIG. 30. Comparison between theory and L.D.V. measurements for $\alpha = 60°$ and 90°, $X = 5$ and $Re = 500$.

pure forced convection case, these two parameters highly affect the size of recirculating zones which develop downstream of the interacting region. For the mixed convection regime, the effect of the Richardson number has also been pointed out. An experimental procedure based upon flow visualization and L.D.V. techniques provides a qualitative and quantitative comparison with the theoretical results. Experimental results confirm the calculated structure flow configurations for both forced and mixed convection regimes.

REFERENCES

1. A Pollard, Computer modelling of flow in tee-junctions, *P s. Chem. Hydrodyn.* **2,** 203–217 (1981).
2. A. Pollard, Flow in tee-junction, Ph.D. Thesis, University of London, Imperial College, Dept of Mech. Engng, Report n° HTS/78/12 (1978).
3. R. M. Blowers, The calculation by finite difference of steady two-dimensional laminar flow in a T-junction, Ph.D. Thesis, University of Surrey (1973).
4. J. S. Bramley and D. M. Sloan, Numerical solution for two-dimensional flow in a branching channel using boundary-fitted coordinates, *Computers Fluids* **15,** 297–311 (1986).
5. R. E. Hayes and K. Nadankumar, Mixed convection heat transfer in a tee branch, *Numer. Heat Transfer* **16,** 287–307 (1989).
6. D. Liepsch, S. Moravec, A. K. Rastogi and N. S. Vlachos, Measurement and calculation of laminar flow in a ninety degree bifurcation, *J. Biomech.* **15,** 473–485 (1982).
7. R. Rieu, R. Pélissier and D. Farahifar, An experimental investigation of flow characteristics in bifurcation models, *Eur. J. Mech. B/Fluids* **8,** 73–101 (1989).
8. T. Karino, H. M. Kwong and H. L. Goldsmith, Particle flow behaviour in models of branching vessels: vortices in 90° T-junction, *Biorheology* **16,** 231–248 (1979).
9. E. M. Sparrow and R. G. Kemink, The effect of a mixing tee on turbulent heat transfer in a tube, *Int. J. Heat Mass Transfer* **22,** 909–917 (1979).
10. Y. Kawashima, M. Nakagawa and S. Iuchi, Heat transfer characteristics in a rectangular flow section downstream from a mixing junction, *Kagaku Kogaku Ronbunshu* **9,** 333–336 (1983).
11. J. C. Roy and G. Le Palec, Convection mixte dans un té convergent, *Int. Com. Heat Mass Transfer* **18,** 49–58 (1991).
12. A. K. Runchal, D. B. Spalding and M. Wolfsthein, The numerical solution of the elliptic equations for transport of vorticity, heat and matter in two-dimensional flows, Imperial College London, Note n° SF/TN/2 (1967).
13. P. J. Roache, *Computational Fluids Mechanics*. Hermosa (1972).
14. A. D. Gosman, W. M. Pun, A. K. Runchal, D. B. Spalding and M. Wolfsthein, *Heat and Mass Transfer in Recirculating Flows*. Academic Press, London (1969).
15. J. P. Prenel, R. Porcar and A. El Rhassouli, Analyse tomographique d'écoulements tridimensionnels par nappe laser en translation, *Optics Comm.* **65,** 101–106 (1988).
16. A. Bejan, *Convection Heat Transfer*. Wiley Interscience (1984).